Biomass measurements of single neurites *in vitro* using optical wavefront microscopy: supplement

LJILJANA DURDEVIC,[1,2] AROA RELAÑO GINÉS,[2] ANTOINE ROUEFF,[1] GUILLAUME BLIVET,[2] AND GUILLAUME BAFFOU[1,*]

[1]*Institut Fresnel, CNRS, Aix Marseille Univ, Centrale Marseille, Marseille, France*
[2]*REGEnLIFE, Montpellier, France*
*guillaume.baffou@fresnel.fr

Supplementary Material

Biomass measurements of single neurites *in vitro* using optical wavefront sensing

Ljiljana Durdevic,[1,2] Aroa Relaño Ginés,[2] Antoine Roueff,[1] Guillaume Blivet[2] and Guillaume Baffou[1,*]

[1]*Institut Fresnel, CNRS, Aix Marseille Univ, Centrale Marseille, Marseille, France*
[2]*REGEnLIFE, Montpellier, France*
*guillaume.baffou@fresnel.fr

1. Estimation of the precision of dry mass measurement.

To estimate the precision of the dry mass measurements, we performed measurements on a series of 10 successive OPD images. Images were acquired at a frame rate of 14.2 Hz, high enough to make sure the measured variations of the dry mass as due to image noise, and not actual mass variations due to cell dynamics.

Different objects of different masses have been selected over le field of view (Figure S1): two objects of a typical dry mass around 3 pg (case 1 and 2), one neurite extremity of less than 1 pg (case 3) and a piece of dust to also quantify the precision on very small objects (case 4).

These data show that a precision of around 0.08 pg is reached for common neurite dry masses of a few pg. For smaller object (case 4), the precision can reach a few fg, making the related precision constant, on the order of a few %.
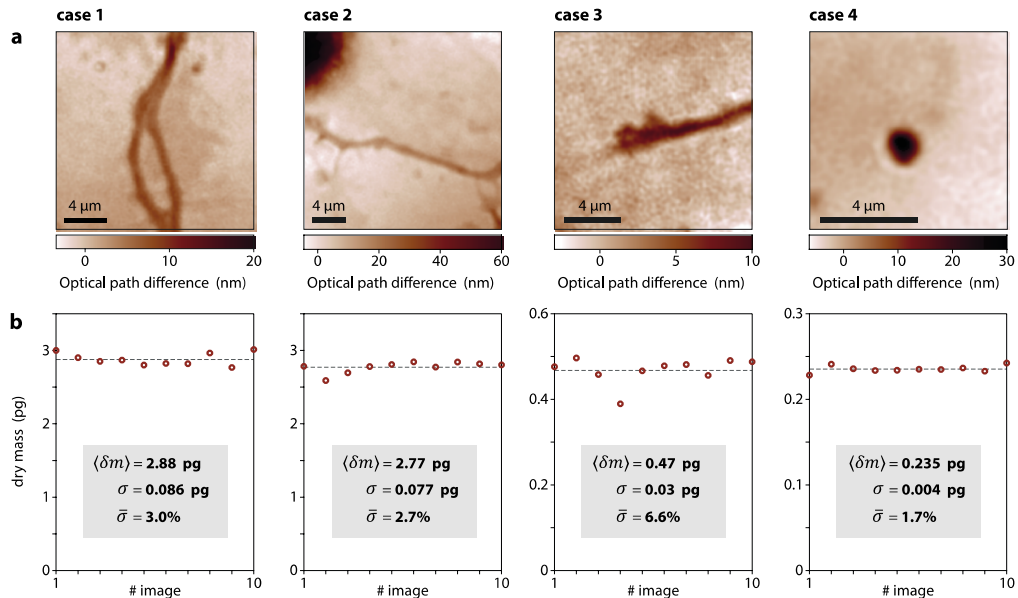

Figure S1: (a) OPD images of 3 neurite sections and one piece of debris. (b) Associated dry mass measurements using the magic wand segmentation algorithm performed on 10 successive images acquired at 14.2 Hz. The average dry mass $\langle \delta m \rangle$ (represented by a dashed line), the standard deviation σ and the normalized standard deviation $\bar{\sigma} = \sigma / \langle \delta m \rangle$ are indicated in the boxes.

In practice, a single reference image is acquired at the beginning of the series of measurements, which can last many days. This is how dry masses of Figure S1 have been measured. Another common way of proceeding in CGM is to take a new reference between each image. We also characterized the precision of this procedure. Figure S2 shows dry mass measurements of a single neurite of 0.36 pg. A comparison is made between the two mode (single reference, and repeated reference). In the repeated-reference mode, the stage was manually moved between each image acquisition, 63 µm from the neurite on a clear area to take a reference image, and then moved back close to the original position. 30 images have been acquired this way. The evolution of the measured dry masses is plotted in Figure S2b. In both cases, a similar average dry mass is measured (0.35 and 0.37 pg), and the standard deviation of the measurements is lower in the single-reference case (0.005 pg, 1.3%), compared with the repeated-reference case (0.013 pg, 3.4%). This trend is expected because variations of the reference images are present in the repeated-reference case.
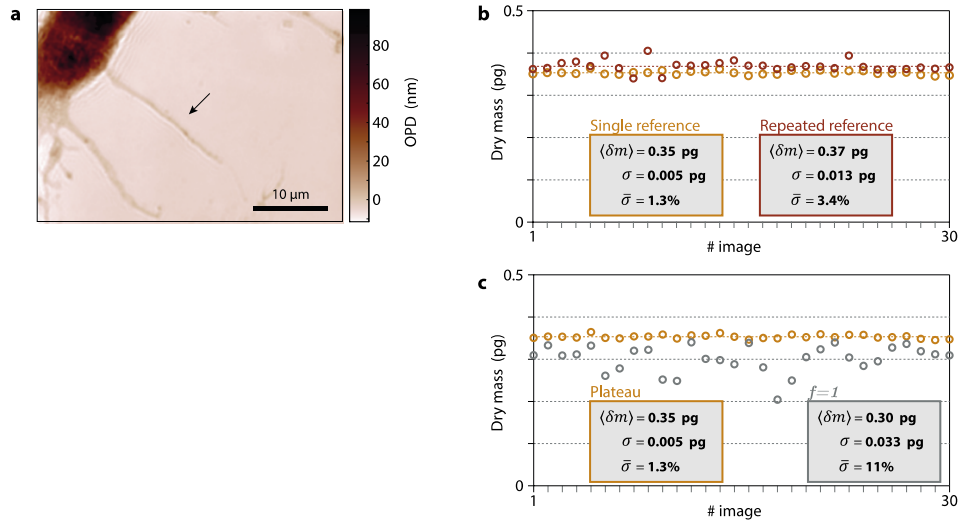

Figure S2: (a) OPD image of a fixed neuron (fixed in PBS). An arrow indicates the selected neuron for dry mass measurements. (b) Measurements of the dry mass of the neuron indicated in (a) on successive OPD images. Orange: a single reference was acquired before the acquisition of a series of 30 images. Red: new reference OPD images (on a clear area, 63 µm away) are repeatedly acquired before each OPD image acquisition. (c) Measurements of the dry mass of the neuron indicated in (a) on successive OPD images (single reference mode). Orange: measurement on the plateau of $\delta V(f)$; Gray: Measurement at $f = 1$.

2. User-dependence

To show that the semi-automatic segmentation algorithm is not significantly user-dependent, two different users performed dry mass measurements on the same series of images, as represented in Figure S3. A very good match is observed.
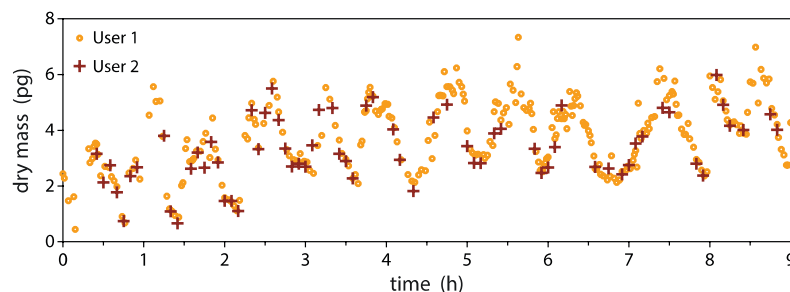
Figure S3. Comparison of dry mass measurements performed on the same series of data by two independent users.

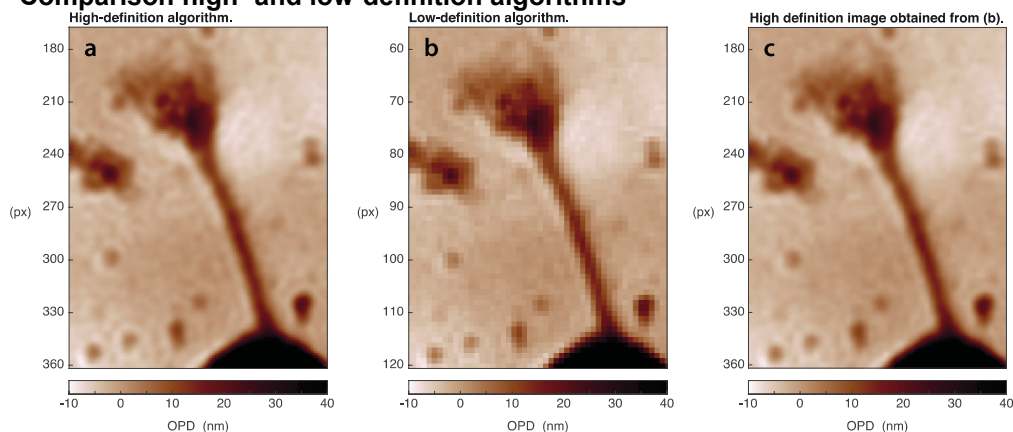## 3. Comparison high- and low-definition algorithms

Figure S4: (a) OPD image of a neurite acquired using a demodulation algorithm (high-definition algorithm) (see doi: 10.1088/1361-6463/abfbf9). (b) Same OPD image obtained using the more common Fourier-crop algorithm (low-definition algorithm). (c) Image obtained from (a) using an image resizing function (Matlab, `resize` function).

Figure S4 illustrates the interest in using the high-definition algorithm (demodulation algorithm) for image rendering. The high-definition algorithm conserves the number of pixels of the camera, unlike the Fourier-crop algorithm that reduces it by a number of 9 to 16. The related algorithm is slower, which can be an issue when implemented in a software for live imaging. However, for data postprocessing and publication of results, we encourage the use of the high-definition algorithm (depicted in doi: 10.1088/1361-6463/abfbf9).

However, although the image definition is higher (more pixels), the spatial resolution remains unchanged. The quantity of information in images (a) and (b) is supposed to be the same. Figure S4c shows the OPD image obtained from (b) using the `resize` function of Matlab, which is quasi-identical to (a). Post-resizing the image is roughly equivalent to using the demodulation/high-definition algorithm (although one can see differences time to time), but it is called 'image postprocessing', while the demodulation algorithm is not, which makes a conceptual difference.

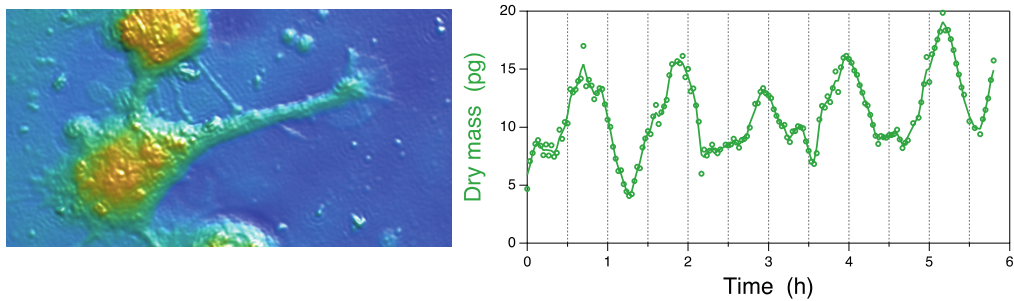## 4. Other examples of neurite oscillation

Figure S5. Example of oscillation of dry mass of a single neurite.

5. Influence of the diffraction rings

In the manuscript, we explain that the diffraction rings are responsible for an underestimated OV when using standard segmentation algorithms. However, on experimental images, these diffraction rings are barely visible due to image noise. To further support this interpretation, we present here OV measurements on simulated OPD images, to discard any image noise and better visualize/confirm the effect of diffraction rings. The simulated OPD image was obtained using IF-DDA (Institut-Fresnel or idiot-friendly DDA), based on the discrete dipole application (DDA), and developed by our colleagues Patrick Chaumet et al. [Chaumet et al. JOSA A 38, 1841 (2021)]. This numerical framework has been developed to simulate images of nano and micro-objects through a microscope. Here, as a simple, illustrative system, we simulated a rod, 3 μm in length and 1.5 μm in diameter. Results are presented in Figure S6. The OPD image exhibits diffraction rings around the rod (see insets of Figure S6). The estimated optical volume as a function of the integration area is plotted. Oscillations are observed, which come from the diffraction rings. These oscillations expand much further than the actual size of the object, and sticking to the actual size of the object leads to an underestimated OV (274 nm^3). One has to go close to $f = 2$ to move away from the oscillation and reach a plateau, leading to a more accurate estimation of the OV. Note that the theoretical OV is straightforward to calculate from simulation images, because the geometry of the object is perfectly known. From the rod-geometry of the bacteria and the refractive index mismatch (1.4 against 1.33), the theoretical OV is

$$OV = \left[4/3\pi(D/2)^3 + \pi(D/2)^2(L-D)\right](n - n_0)$$

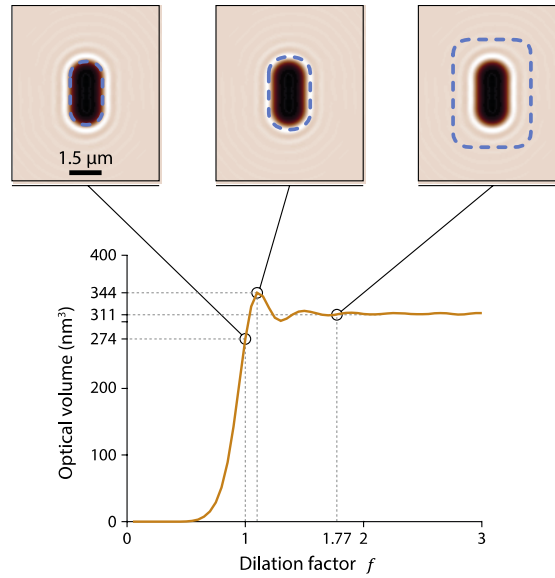where gives OV=310 nm^3, exactly the limit value in Figure S6.

Figure S6. Segmentation algorithm applied on a simulated OPD image of a dielectric rod, $L = 3$ μm in length, $D = 1.5$ μm in diameter, $n = 1.4$, in water ($n_0 = 1.33$), and deposited on glass ($n_S = 1.51$). $\lambda = 550$ nm. Objective magnification $100 \times$, 1.3 NA. The estimated optical volume is plotted as a function of the dilation factor f. Three specific f values are highlighted, along with the corresponding integration boundaries on the insets (dashed blue lines).

6. Movie and time lapse

Movie M1.avi displays the OPD of the sequence acquired for 15 hours corresponding to Figure 4 of the main article. In addition to the movie, a time lapse is given on the next page.
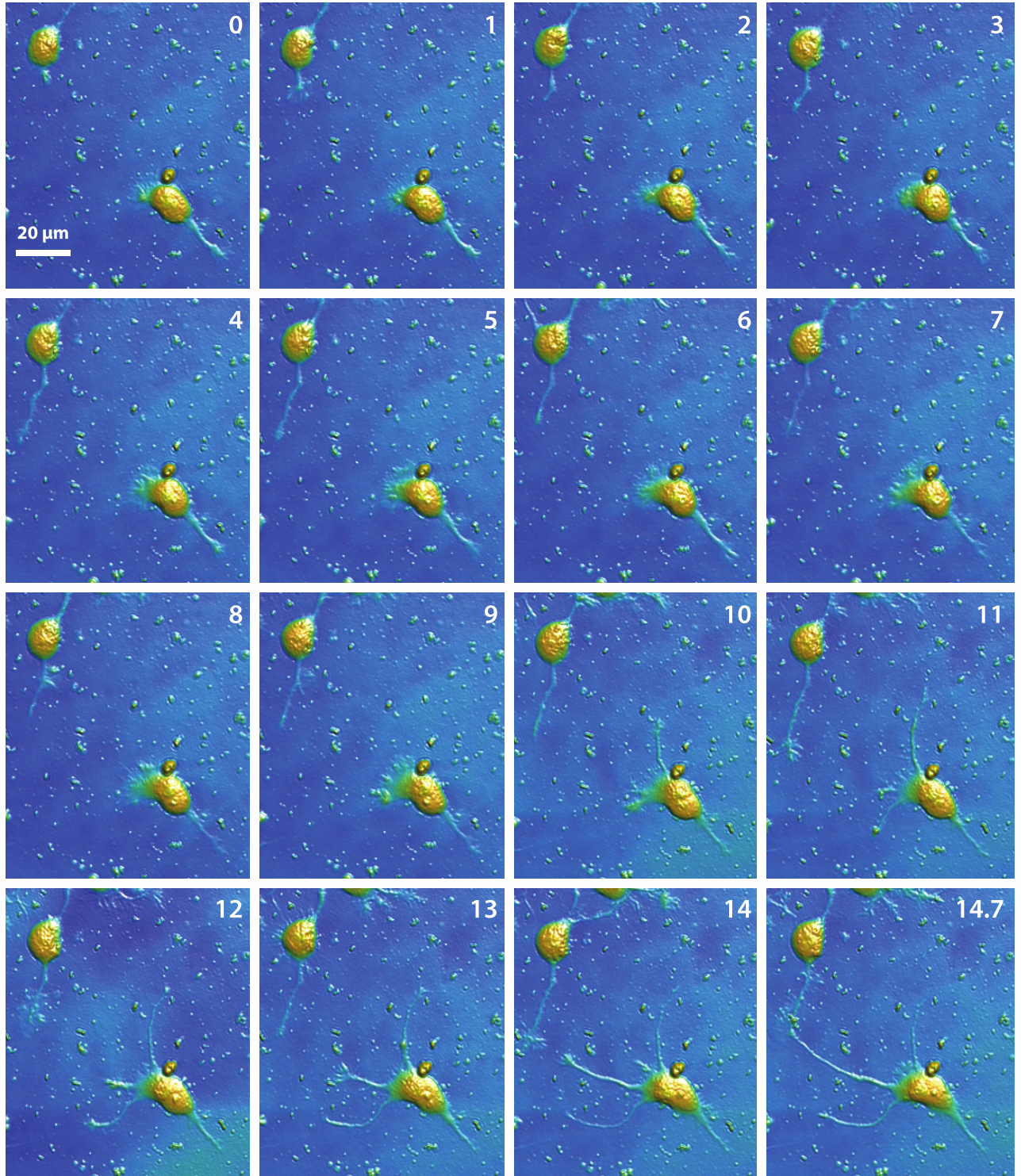
Figure S7 Time lapse of the series of measurements associated with Figure 4 and Movie M1.